



Pietro Caprioglio | Martin Stolterfoht | Christian M. Wolff
Thomas Unold | Bernd Rech | Steve Albrecht | Dieter Neher

On the Relation between the Open-Circuit Voltage and Quasi-Fermi Level Splitting in Efficient Perovskite Solar Cells

Suggested citation referring to the original publication:
Advanced Energy Materials 9 (2019) 33, Art. 1901631
DOI <https://doi.org/10.1002/aenm.201901631>
ISSN (print) 1614-6832
ISSN (online) 1614-6840

Postprint archived at the Institutional Repository of the Potsdam University in:
Postprints der Universität Potsdam
Mathematisch-Naturwissenschaftliche Reihe ; 774
ISSN 1866-8372
<https://nbn-resolving.org/urn:nbn:de:kobv:517-opus4-437595>
DOI <https://doi.org/10.25932/publishup-43759>

On the Relation between the Open-Circuit Voltage and Quasi-Fermi Level Splitting in Efficient Perovskite Solar Cells

Pietro Caprioglio, Martin Stolterfoht, Christian M. Wolff, Thomas Unold, Bernd Rech, Steve Albrecht, and Dieter Neher*

Today's perovskite solar cells (PSCs) are limited mainly by their open-circuit voltage (V_{OC}) due to nonradiative recombination. Therefore, a comprehensive understanding of the relevant recombination pathways is needed. Here, intensity-dependent measurements of the quasi-Fermi level splitting (QFLS) and of the V_{OC} on the very same devices, including pin-type PSCs with efficiencies above 20%, are performed. It is found that the QFLS in the perovskite lies significantly below its radiative limit for all intensities but also that the V_{OC} is generally lower than the QFLS, violating one main assumption of the Shockley-Queisser theory. This has far-reaching implications for the applicability of some well-established techniques, which use the V_{OC} as a measure of the carrier densities in the absorber. By performing drift-diffusion simulations, the intensity dependence of the QFLS, the QFLS- V_{OC} offset and the ideality factor are consistently explained by trap-assisted recombination and energetic misalignment at the interfaces. Additionally, it is found that the saturation of the V_{OC} at high intensities is caused by insufficient contact selectivity while heating effects are of minor importance. It is concluded that the analysis of the V_{OC} does not provide reliable conclusions of the recombination pathways and that the knowledge of the QFLS- V_{OC} relation is of great importance.

photoluminescence yields (>20%).^[5] In principle, this would allow open-circuit voltages (V_{OC}) very close to the radiative limit (≈ 1.3 V for a bandgap of 1.6 eV) using already existing perovskites. However, despite the tremendous effort devoted by the scientific community on the improvement of this solar cell technology, the experimental efficiencies are still far from the Shockley-Queisser (S.Q.) theoretical predictions of power conversion efficiency (PCE) up to 30%.^[6] Specifically, in order to further improve the PCE, the effort must be focused on increasing the V_{OC} and the fill factor (FF) through the reduction of nonradiative recombination losses. Moreover, a better understanding on the predominant energy loss mechanisms in the working device has to be accomplished.


Perovskite solar cells generally consist of a 300–500 nm layer of photoactive absorber, sandwiched between two charge transporting layers that have the function of selectively transporting the photo-

generated electrons (holes) to the cathode (anode). In an ideal solar cell, all photons are absorbed in the perovskite films, generating electrons and holes with unity efficiency, and—under open-circuit conditions—the only recombination channel is the radiative recombination of free electrons and holes in the same layer where they are generated. Commonly, reported values for V_{OC} are much lower due to unwanted nonradiative recombination. During the past years, many studies have evaluated recombination in perovskites layers and suggested that defects at the perovskite surface or at grain boundaries as possible reasons

1. Introduction

With astonishingly high efficiencies and low-cost production, perovskite solar cells have the potential to become a leading technology in the photovoltaic sector. The underlying reason for this rapid success is rooted in their high absorption coefficient, panchromatic absorption of light,^[1] long carrier diffusion length^[2,3] and shallow trap energy levels.^[4] The combination of these properties allows for a high photocurrent and low non-radiative recombination with exceptionally high (external)

P. Caprioglio, Dr. M. Stolterfoht, C. M. Wolff, Prof. D. Neher
Institut für Physik und Astronomie Physik weicher Materie
University of Potsdam
14476 Potsdam, Germany
E-mail: neher@uni-potsdam.de

 The ORCID identification number(s) for the author(s) of this article can be found under <https://doi.org/10.1002/aenm.201901631>.

© 2019 The Authors. Published by WILEY-VCH Verlag GmbH & Co. KGaA, Weinheim. This is an open access article under the terms of the Creative Commons Attribution License, which permits use, distribution and reproduction in any medium, provided the original work is properly cited.

The copyright line for this article was changed on 23 August 2019 after original online publication.

DOI: 10.1002/aenm.201901631

P. Caprioglio, Prof. S. Albrecht
Young Investigator Group Perovskite Tandem Solar Cells
Helmholtz-Zentrum Berlin für Materialien und Energie GmbH
12489 Berlin, Germany

Dr. T. Unold
Helmholtz-Zentrum Berlin für Materialien und Energie GmbH
14109 Berlin, Germany

Prof. B. Rech
Institute for Silicon Photovoltaics
Helmholtz-Zentrum Berlin für Materialien und Energie GmbH
12489 Berlin, Germany

Prof. B. Rech, Prof. S. Albrecht
Faculty IV—Electrical Engineering and Computer Science
Technical University Berlin
10587 Berlin, Germany

for nonradiative recombination in neat perovskite layers.^[7–10] More recently, several studies have additionally highlighted the thorny problematic of the interfaces between the perovskite and charge transport layers in the actual device, due to the fast nonradiative recombination of carriers at or across these interfaces.^[11–14] Therefore, a detailed understanding of the losses and the underlying physical processes is essential in order to exploit the full potential of these materials in solar cells.

A common approach to study the rate and mechanisms of recombination is to measure specific recombination properties, such as the carrier lifetime or the recombination current density, as a function of the V_{OC} .^[15–18] Hereby, the V_{OC} is used as a measure of how strongly the carrier distribution of the illuminated sample differs from the thermal equilibrium. For example, the recombination current is commonly written in terms of the classical diode equation

$$J_R = J_0 \cdot e^{\left(\frac{qV_{OC}}{n_{id}k_B T}\right)} \quad (1)$$

Here, J_0 is the total dark recombination current due to radiative and nonradiative processes, while n_{id} is the ideality factor, which describes the deviation from the ideal diode condition where only pure bimolecular recombination is considered. However, the V_{OC} is a quantity measured externally, at the device's *external* contacts and given the multilayer architecture of the perovskite solar cells it might be not truly representative of the quasiequilibrium established in the absorber or at the absorber/transport layer interfaces. On the other hand, an *internal* quantity representative of the density of free photogenerated charges in the conduction band (CB) and valence band (VB) of the absorber is the quasi-Fermi level splitting (QFLS). In the S.Q. theory, the QFLS and the V_{OC} are two interchangeable quantities which are considered as equal to each other.^[19,20] However, it has been experimentally observed that the magnitude of the *internal* QFLS is not always equal to the *external* V_{OC} .^[12] Moreover, several authors reported that the V_{OC} saturates at high illumination intensities (>1 sun), which is of particular importance for applications of perovskite in solar cell concentrators.^[21] While several mechanism have been proposed to explain the V_{OC} saturation,^[15,22,23] it still constitutes a matter of active debate. On the other hand, there are very few publications regarding the intensity dependence of the QFLS, and none of these reported a saturation of the QFLS.^[24]

In this work, we compare the *external* V_{OC} with the *internal* QFLS of the same solar cell device, obtained using photoluminescence quantum yield (PLQY) measurements. We monitor the evolution of the two quantities with respect to the light intensity. From these data, we calculate two different ideality factors, namely an *internal* ideality factor, obtained from the QFLS measurements, and an *external* ideality factor, obtained from the V_{OC} measurements. The study is performed on two different perovskite solar cell model systems characterized by different energy losses and utilizing different hole transporting layers (HTL), namely poly[bis(4-phenyl)(2,4,6-trimethylphenyl)amine] (PTAA), and poly(3-hexylthiophene-2,5-diyl) (P3HT). For both systems, the QFLS increases continuously with light intensity, with a constant *internal ideality* factor of ≈ 1.3 – 1.5 , while the V_{OC} displays a clear saturation for both types of

devices. We also find that the V_{OC} of the poorer performing device lies significantly below the QFLS for all light intensities. This finding challenges the common view that the V_{OC} is a proper measure of the deviation from thermal equilibrium of the illuminated system. Therefore, the measurements of the V_{OC} as function of intensities do not allow to draw reliable conclusions about the mechanism of recombination. By implementing drift-diffusion simulations, we elucidate the possible causes for the V_{OC} saturation and identify its limitations, compared to the QFLS potentially achievable.

2. Theory

The quasi-Fermi levels $E_{F,e}$ and $E_{F,h}$ are quantities representing the density of the free photogenerated electron (holes) in the conduction (valence) band, in the limit of quasiequilibrium (note that $E_{F,e}$ and $E_{F,h}$ are alternatively written as $E_{F,C}$ and $E_{F,V}$, where “C” stands for the conduction band and “V” for the valence band). The difference between $E_{F,e}$ and $E_{F,h}$ is the QFLS. While the absolute locations of $E_{F,e}$ and $E_{F,h}$ are generally not accessible, the QFLS can be determined directly by means of absolute PL measurements.^[16,19,20,25,26] This methodology has been proven to be an efficient approach for quantifying recombination losses in the neat perovskite, multilayer assemblies or even complete perovskite solar cells.^[11,24,27,28]

This method relies on the assumption, that all photoluminescence (PL) stems from the radiative recombination of free charges in the perovskite. Then, the quantum yield of the PL radiation is the ratio between the emitted photon flux ϕ_E from free carrier recombination on the perovskite and the absorbed photon flux ϕ_A or, equivalently, as the ratio between the total radiative recombination current J_{rad} and the generation current J_G

$$PLQY = \frac{\phi_E}{\phi_A} = \frac{J_{rad}}{J_G} = \frac{J_{rad}}{J_R} = \frac{J_{rad}}{J_{rad} + J_{non-rad}} \quad (2)$$

At V_{OC} conditions, the net current flowing in the device is zero and J_G is equal to the recombination current J_R , which consists in the radiative (J_{rad}) component and all nonradiative recombination processes ($J_{non-rad}$) in the perovskite and all other layers and interfaces. On the other hand, for quasi equilibrium under steady state illumination, the density of free carriers in the valence and conduction band of the perovskite is related to the QFLS (or the sum of the chemical potentials of free electron-hole pair, μ) as follows^[19]

$$n^2 = N_c N_v \cdot e^{\left(\frac{E_c - E_v}{k_B T}\right)} \cdot e^{\left(\frac{E_{F,e} - E_{F,h}}{k_B T}\right)} = n_i^2 \cdot e^{\left(\frac{QFLS}{k_B T}\right)} \quad (3)$$

where N_c and N_v are the effective density of states in the conduction band and the valence band respectively, T is the temperature, k_B is the Boltzmann constant, E_c and E_v are the conduction and valence band energy levels respectively, n_i is the intrinsic carrier density in the dark and QFLS represents the splitting of the quasi-Fermi levels. We relate now Equation (3) to the radiative recombination current $J_{rad} = edR = edkn^2$, which is the current originated exclusively from bimolecular radia-

tive recombination in the perovskite, and to the dark radiative recombination current $J_{0, \text{rad}} = edkn_i^2$, which is the current due to radiative recombination of carriers in the dark. The latter is related to the absorption of the background black body radiation by the detailed balance principle.^[20,29] Then

$$J_{\text{rad}} = J_{0, \text{rad}} \cdot e^{\left(\frac{\text{QFLS}}{k_B T}\right)} \quad (4)$$

Furthermore, Equation (4) can be combined with Equation (1) to arrive at a direct relation between the PLQY and the QFLS

$$\begin{aligned} \text{QFLS} &= k_B T \cdot \ln\left(\frac{J_{\text{rad}}}{J_{0, \text{rad}}}\right) = k_B T \cdot \ln\left(\text{PLQY} \frac{J_G}{J_{0, \text{rad}}}\right) \\ &= \text{QFLS}_{\text{rad}} + k_B T \cdot \ln(\text{PLQY}) \end{aligned} \quad (5)$$

Here, QFLS_{rad} is the radiative limit of our semiconducting material, setting the maximum achievable splitting of the quasi-Fermi levels, hence the V_{OC} , in the case of zero nonradiative recombination. Generally, PLQY under steady state illumination conditions will be limited by all recombination processes, meaning that there is no trivial relation between the QFLS and J_G . However, within a limited intensity interval, this relation can be written in terms of a modified diode equation^[24]

$$J_G = J_R = J_0 \cdot e^{\left(\frac{\text{QFLS}}{n_d k_B T}\right)} \quad (6)$$

While this equation looks similar to Equation (1), there is an important difference between the QFLS and qV_{OC} . While QFLS is the difference of the electron and hole quasi-Fermi levels in the perovskite layer, qV_{OC} stands for the difference of $E_{F,e}$ at the cathode and $E_{F,h}$ at the anode. Only when there is no bending of the quasi-Fermi levels and each of them aligns with the respective electrode work function, then $\text{QFLS} = qV_{\text{OC}}$. We will show below that this situation does not hold in general for perovskite-based solar cells, meaning that the V_{OC} should not be considered when aiming to a proper analysis of the recombination currents, in terms of carrier densities in the absorber.

3. Experimental Results

Two pin-type perovskite solar cells with the so called “triple cation” $\text{Cs}_{0.05}(\text{MA}_{0.17}\text{FA}_{0.83})_{0.95}\text{Pb}(\text{I}_{0.83}\text{Br}_{0.17})_3$ perovskite absorber^[30] and two different semiconducting polymers as HTLs, namely P3HT and PTAA, are compared in Figure 1a. Consistent with our previous reports,^[12,31] the PCE of our P3HT cells is lower compared to the cells with a PTAA hole transporting layer, which regularly exhibit PCEs exceeding 20%.^[11] Most of the limitation comes from the poor V_{OC} s of below 1 V when utilizing P3HT, while PTAA cells generally exhibit V_{OC} s of 1.14 V and above, depending on the choice of the perovskite and electron transporting material. The reduction in J_{SC} for P3HT cells is due to its energy gap (E_g) of roughly 2 eV, which allows absorption of light overlapping with the perovskite absorption, consequently reducing the number

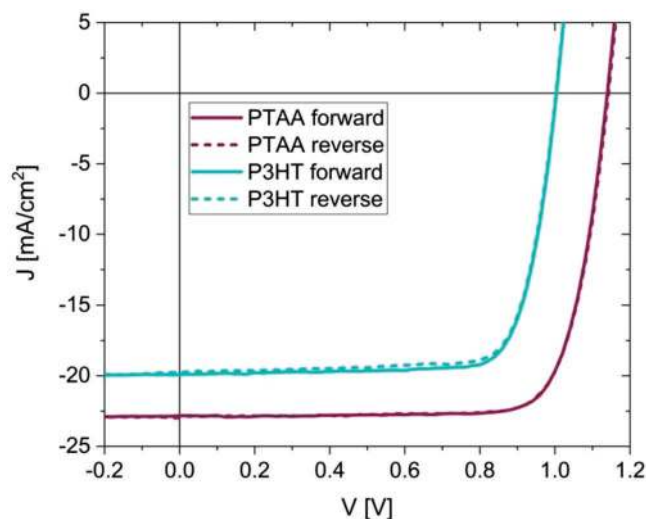


Figure 1. J - V characteristics of forward and reverse scans (0.1 V s^{-1} with voltage step of 0.02 V) under simulated AM 1.5G illumination calibrated to 100 mW cm^{-2} for two typical devices utilizing PTAA and P3HT as hole transporting layers.

of photons reaching the perovskite absorber. We also note a slightly reduction of the FF, which we will address further below. All the relevant values are reported in Table 1.

To study the energy losses in detail, we performed intensity-dependent PL and V_{OC} measurements on the very same solar cell device. The PLQY was measured by exciting the complete device, inside an integrated sphere with a 455 nm laser diode, varying its intensity. The V_{OC} was measured with the very same light source, in the same intensity regime. The laser intensity is normalized to 1 sun when the illuminated cell shows a current density at 0 V equal to the J_{SC} . Importantly, the PLQY, as the calculated QFLS, is an internal quantity, which represent the destiny of the photogenerated charges recombining in the absorber or its interfaces; on the other hand the V_{OC} is quantity measured at the external contact, therefore taking into account also the possible recombination processes happening in the transport layers or at the contacts. The dependence of the PLQY on the illumination intensities is presented in Figure 2. In the ideal case of purely radiative recombination, the PLQY is independent of illumination intensity. Instead, both cells show an intensity dependence according to the power law $PL(I) \propto I^k$, suggesting that nonradiative recombination processes of lower order, most likely assisted by traps in the perovskite bulk, at grain boundaries or at the interfaces, compete with the second order radiative recombination of free carriers as described by Equation (2).^[35] The larger slope for the lower performing cell with P3HT highlights the importance of this process in limiting the efficiency of our cells.

Table 1. J - V parameters for the two model devices taken from J - V scans and averaged over 10 cells. Inside the brackets, values for the champion device are reported.

	V_{OC} [V]	J_{SC} [mA cm^{-2}]	FF [%]	PCE [%]
P3HT	0.95 ± 0.04 (0.98)	20.4 ± 0.5 (21.2)	73 ± 4 (78)	14.2 ± 1.2 (16.23)
PTAA	1.14 ± 0.01 (1.15)	22.2 ± 0.6 (22.9)	77 ± 2 (78)	19.4 ± 0.6 (20.56)

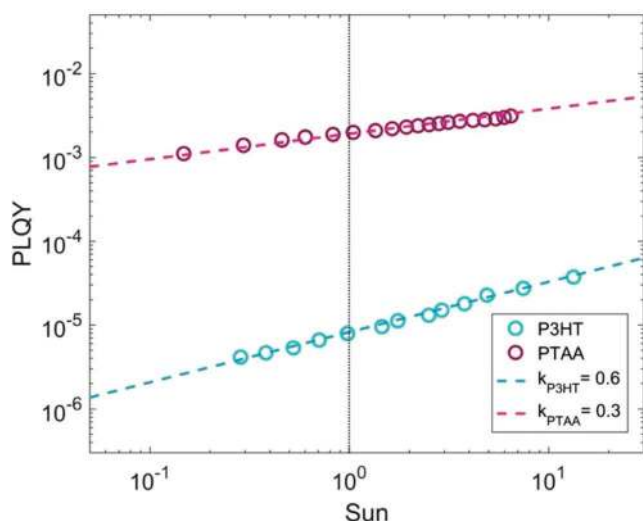


Figure 2. Intensity-dependent photoluminescence quantum yield (PLQY) measured on two cells with P3HT and PTAA as hole transport layer, respectively. The PLQY is generally higher for the PTAA case, indicating less nonradiative losses for this system.

To calculate the *internal* QFLS via Equation (5), the radiative limit of the QFLS, $QFLS_{rad}$, was calculated according to the approach presented in Section 1 (Supporting Information). The result is compared with the corresponding $QFLS_{rad}$ and the V_{OC} of the same cell in **Figure 3a**). Several important findings can be discerned. First, the measured QFLS as function of intensity (I) lies significantly below $QFLS_{rad}(I)$ over the entire intensity range and increases with a higher slope. This is also expressed by an $n_{id} > 1$ (compared to $n_{id} = 1$ for $QFLS_{rad}(I)$). Notably, the

difference in the overall magnitude is significantly larger for the poorer performing device, which consistently exhibits a larger ideality factor. Second, for low to intermediate intensity, depending on the system, $qV_{OC}(I)$ and $QFLS(I)$ increase with similar slopes. Notably, in this intensity range, the PTAA cell shows a good match ($<10\text{meV}$) between V_{OC} and the QFLS, while for the P3HT cell, $qV_{OC}(I)$ remains below $QFLS(I)$ by at least 80 meV. When increasing the intensity further, for both devices the $qV_{OC}(I)$ starts to saturate, while the $QFLS(I)$ continues to follow the initial trend. Interestingly, the onset of the saturation is significantly different for the two samples. For all intensities considered here, the difference between QFLS and the qV_{OC} is, however, smaller than the loss in QFLS compared to its radiative limit, limiting the V_{OC} to significantly below its radiative limit even for the well performing device. Overall, the measurements of the QFLS and V_{OC} on the same sample reveal important differences between these two quantities, in particular at higher illumination intensities. This questions the accuracy of well-established characterization methodologies which make use of the intensity dependence of the V_{OC} as representative of the carrier concentration inside the absorber. In the following, we will go step-by-step through the processes determining the intensity dependence of QFLS and V_{OC} , and conclude with the overall recombination picture of the device at different illumination intensities.

3.1. Quasi-Fermi Level Splitting

It is well established that the QFLS of state-of-the-art perovskite solar cells still lies well below the $QFLS_{rad}$. According to Equation (5), this is due to nonradiative losses, e.g.,

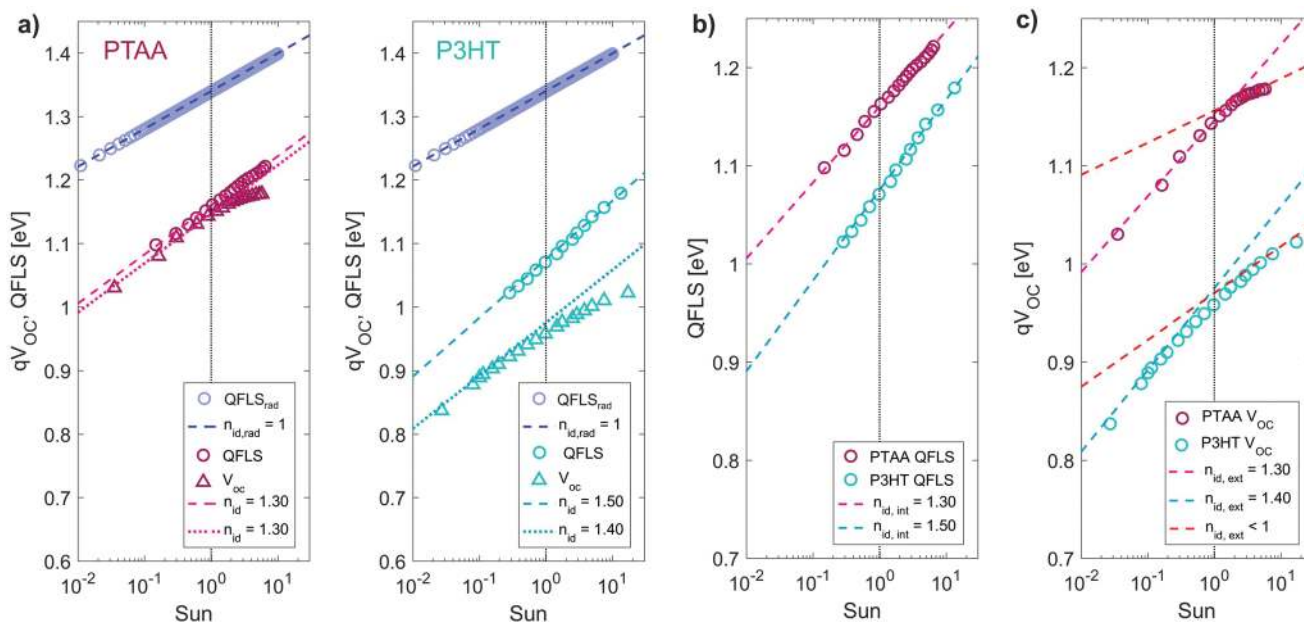


Figure 3. a) Comparison between qV_{OC} , QFLS, and $QFLS_{rad}$ of the corresponding solar cell using PTAA and P3HT as HTL, respectively. The V_{OC} is directly measured, the QFLS is obtained from PLQY measurements through Equation (5), and the $QFLS_{rad}$ is calculated analogously but assuming $PLQY = 1$. The $V_{OC}(I)$ measurements were performed on the same solar cell sample, illuminating the sample at exactly the same illumination intensity and light exposure as in the case of PL measurements. b) Internal ideality factor calculated from the dependence of the QFLS on illumination intensity and c) external ideality factor calculated from the dependence of the V_{OC} on illumination intensity.

nonradiative recombination in the bulk and at interfaces and/or parasitic absorption.^[24,32,33] A possible way to look at the nature of these losses is to study the ideality factor.^[15] By definition, an ideality factor equal to 1 refers to only second order bimolecular recombination of free charges whereas, an ideality factor close to 2 is explained by a first order monomolecular recombination processes, e.g., symmetric trap-assisted recombination through mid-gap traps.^[34] Perovskite solar cells generally exhibit values between these extremes. This is usually indicative of a superposition of first and second order recombination mechanism, involving monomolecular and bimolecular recombination.^[35] There are two observations speaking against this interpretation. First, the competition between a first and a second order loss would be in favor for the first (second) order process at low (high) intensities, rendering n_{id} to be a function of intensity. This is in clear contrast to our observation that the measured QFLS(I) has a constant slope throughout the entire intensity range. Second, the PLQY remains well below 1% for both devices at even the highest intensity, meaning that radiative recombination is of minor importance. We, therefore, conclude that the recombination in our devices is dominated by one particular pathway, that this pathway is nonradiative, and that it is more efficient in the case of P3HT. Recently, $n_{id} = 1.5$ was attributed to nonradiative trap-assisted recombination where free holes recombine predominately with trapped electrons (but not the other way around).^[36–38] Our analysis of QFLS(I) with Equation (6) yields $n_{id,int} = 1.30$ and 1.50 for the device with PTAA and P3HT, respectively (we refer to the ideality factor obtained from QFLS as *internal* ideality factor, $n_{id,int}$). These values are below the above prediction of the recombination of free holes with trapped electrons, and they are distinctly different for the two hole transporting materials. We will show below that our experimental findings are consistent with a model, where recombination of photogenerated charges is predominately across the perovskite/CTL interfaces.

3.2. Open-Circuit Voltage

At low to intermediate intensities, QFLS(I) increases almost in the same way as $qV_{OC}(I)$, meaning that $n_{id,ext} \cong n_{id,int}$ (here we denote the ideality factor from V_{OC} as the *external* ideality factor, $n_{id,ext}$). In the case of PTAA the two ideality factors perfectly match, indicating that both V_{OC} and QFLS are determined by the very same recombination mechanism. On the other hand, in the P3HT case, the $n_{id,ext}$ is always a bit lower than the $n_{id,int}$ and qV_{OC} lies always below QFLS. This means that this recombination loss must occur predominately in the vicinity of the perovskite surfaces or near the electrodes, and it is stronger than in the bulk. In a previous study we have explained this finding by an energetic offset between the highest occupied molecular orbital (HOMO) (lowest occupied molecular orbital (LUMO)) of the hole (electron) transporting material and the VB (CB) of the perovskite in conjunction with rapid interfacial recombination.^[12] As a result, the density of majority carriers in the perovskite becomes reduced specifically near the respective contacts, causing an upward (downward) bending of $E_{F,h}$ ($E_{F,e}$), which finally reduces V_{OC} compared to the QFLS in the perovskite bulk. We note that the exact interfacial offset is

not known to us for the studied system, as we have no access to the energetics at buried interfaces.

In both samples, at high densities, the V_{OC} starts to saturate and the internal and external ideality factors deviate. The V_{OC} saturation phenomena has been observed for different type of solar cells, but a common consensus regarding its causes has not been reached in the community.^[15,22,23] Recent studies pointed out that the saturation of the V_{OC} can be explained by an increase in local temperature under high illumination conditions.^[39] However, several of our experimental findings disprove this model. First, measurements of the $V_{OC}(I)$ at different conditions, namely with and without temperature controller, and with different illumination exposure times, yielded the same results, see Figure S2A,B (Supporting Information). We also monitored the local temperature increase with an infrared sensor at the laser incident spot, which showed an only modest increase at 10 suns, regardless of the presence of the temperature controller. This indicates that the metal sample holder that carries the substrate ($2.5 \times 2.5 \text{ cm}^2$) acts as a heat sink and it is sufficient to dissipate efficiently the heat produced by the rather small illumination spot of $\approx 3 \times 3 \text{ mm}^2$. Furthermore, from the PL spectra taken at different illumination conditions, it is possible to calculate the local temperature of the emissive volume,^[5,25,28] as presented in Figure S2C (Supporting Information). These data lack evidence for an appreciable increase in temperature when increasing the illumination intensity from 0.1 to 10 suns during the short illumination time ($\approx 1 \text{ s}$). Finally, and most importantly, QFLS(I) exhibits a constant slope at even the highest intensity range. Given that the illumination conditions are the same when measuring $V_{OC}(I)$ and QFLS(I) on the same sample, and that $n_{id,ext} = n_{id,int}$ at intermediate intensities, Equations (4) and (6) predict the very same effect of temperature on QFLS(I) and $V_{OC}(I)$, which is apparently not the case. We conclude that the saturation of the V_{OC} has to be caused by an additional nonradiative recombination loss, which specifically affects the V_{OC} , meaning this process occurs (again) near the perovskite surface and electrodes.

3.3. Recombination Pathways

In order to shed more light on this matter, we perform one dimensional drift-diffusion simulations to model our two typical perovskite devices at different illumination conditions, using realistic solar cell parameters. The simulation relies on the model outlined in Stolterfoht et al.^[12] This includes our complete multilayer stacks, with specific carrier lifetime and specific interface recombination velocities at the interfaces, implemented with mid-gap traps. To keep the number of fit parameters as small as possible, most of them were set constant using reasonable values from the literature or from our own simulation work. Table S1 (Supporting Information) lists the final set of values, including the parameters that were kept variable to fit the data. This simple model gave a fairly good fit of the observed QFLS(I) and $V_{OC}(I)$ data at low and intermediate intensity, but we were not capable to explain the saturation of the V_{OC} (and the lack of the QFLS saturation) at high intensity. We found out that in order to reproduce the V_{OC} saturation it is necessary to add a new recombination pathway

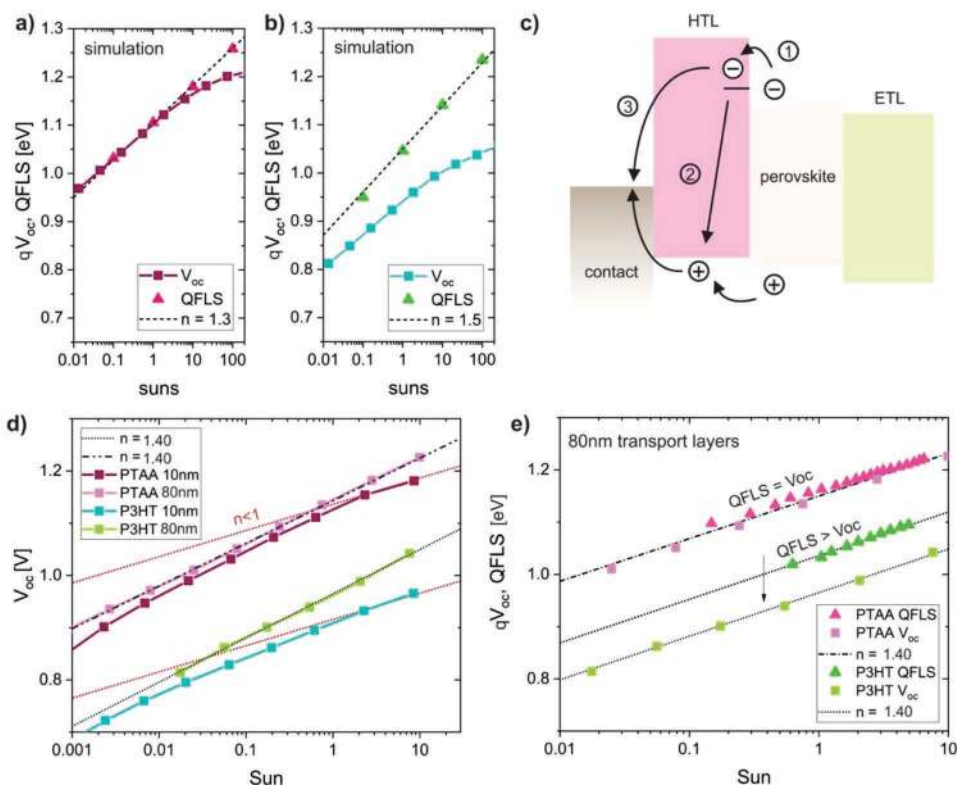


Figure 4. Intensity-dependent drift-diffusion simulation results for two different solar devices utilizing a) PTAA and b) P3HT using the first saturation model. c) Schematic representation of the possible recombination processes that cause the V_{OC} saturation. 1) Electrons can reach the HTL either by additional high-energy interfacial states or by the lack of selectivity of the HTL at certain points of the substrate. Consequently, the electrons on the HTL now can recombine with the holes in the HTL (2) or they can reach the contacts and undergo recombination there with the holes trying to reach the external circuit (3). d) Experimental results of the effect of the HTL thickness on the $V_{OC}(I)$ and ideality factor measurements. e) Experimental results of the QFLS(I) and $V_{OC}(I)$ comparison for solar cells using 80 nm PTAA and P3HT respectively as HTL.

that becomes relevant exclusively at sufficiently high minority carrier density. To account for this, we added a further trap at the perovskite/HTL interface, located above (or at) the perovskite CB, outside its bandgap. This situation is presented schematically in Figure S3A (Supporting Information). In the limit that the filling and detrapping of this state are faster than its draining through recombination with a hole on the HTL, the trap occupation, n_T , follows the Fermi–Dirac statistic, meaning that the density of occupied traps is nearly proportional to the electron density (minority carrier density) at the interface: $n_T \propto n_e$. Then, with an intensity-dependent hole density at the interface, $n_h(I)$, the rate of interfacial recombination becomes $R(I) \propto n_h(I) \times n_T \propto n_h(I) \times n_e(I)$, meaning that it is a higher order process. In fact, when we conduct simulations with only the new recombination channel being active, we get an $n_{id} = 1.2$, which is fairly close to the $n_{id} = 1$ obtained with exclusively radiative second order recombination

For the PTAA cell, this model gives an excellent fit to the experimental results, matching nicely the internal and external ideality factors $n_{id,ext} \cong n_{id,int} = 1.3$, as well as the onset and extent of the V_{OC} saturation (Figure 4a). Interestingly, when in the simulation model the additional recombination channel is deactivated for the PTAA cell, Figure S3D (Supporting Information), the QFLS and the V_{OC} matches throughout all the intensity range, with $n_{id,ext} \cong n_{id,int} = 1.4$. A detailed analysis of the rates and internal currents reveals that most recombination

proceeds through interfacial states and is nonradiative. As such, an ideality factor of 1.4 is neither characteristics for the competition between radiative ($n_{id,int} = 1$) and trap-assisted ($n_{id,int} = 2$) recombination, nor it allows conclusions about the nature and energy of traps inside the perovskite. Instead, we find that the value of n_{id} depends mainly on the energetics at the interface and the related capture rates for carriers at both side of the heterojunction. A detailed study on these dependencies will be published separately. For the P3HT device, we add an energetic offset of 0.2 eV between the HOMO of the HTL and the VB of the perovskite in order to reproduce the QFLS- V_{OC} mismatch at low-intermediate intensities.^[12] Also, the position of the additional trap state was moved closer to the perovskite CB. This increases the effectiveness of this additional recombination path and leads to an earlier onset of the saturation of the V_{OC} . Additional simulation show how varying the position and the recombination velocity of these trap states is determinant for the onset and degree of V_{OC} saturation, see Figure S3B (Supporting Information). We note here that when the additional trap is removed, the difference between the V_{OC} and the QFLS is maintained due to the majority carrier offset. Here, a modest difference between $n_{id,ext}$ and $n_{id,int}$ is still present. As expected, the implementation of this additional recombination channel has also an overall effect on the QFLS, generally lowering it when active, Figure S5d (Supporting Information). Interestingly, the difference is more pronounced in the

PTAA case, where also a change in slope is observed, compared to the P3HT where the strong surface recombination due to the energetic offset is alleviating the effect of the new channel.

Independent of these details, the very good agreement of the simulation results and the experimental data suggests the presence of a recombination channel that allows electrons to enter the HTL via states that are close to the CBM, as schematically represented in Figure 4c). This is equivalent to the situation of a contact with reduced selectivity. We, therefore, modelled a second situation where the contact is completely nonselective. As presented in Figure S4A,B (Supporting Information), in this scenario, the minority carriers are able to directly enter the HTL and to recombine with the majority carrier either at the contacts or in the HTL. In this extreme case, the V_{OC} is limited by the work function difference between the two metal contacts, i.e., the built-in field. A similar picture has been already proposed in the case of silicon solar cells, where back contact recombination has been introduced and modelled as an opposite diode activated only at sufficiently high carrier density.^[22] While this model can explain the V_{OC} saturation, the complete unselectivity of the HTL implemented in our simulation represents an over exaggerated scenario that leads to too low V_{OC} s compared to our devices.

These results suggest a third option, namely that the non-ideal coverage provided by the very thin HTL layer (<10 nm) introduces an additional direct recombination channel between the contact and the perovskite, gradually becoming stronger at high illumination intensities. Motivated by the results of the simulations, we measured the QFLS(I) and $V_{OC}(I)$ on cells with different HTLs thickness, as shown in Figure 4d,e. The usage of thicker transport layers totally prevents the saturation of the V_{OC} across the whole intensity range of the experiment. The *external* ideality factor from the $V_{OC}(I)$ is constant and approaches the same values of the *internal* one for both systems. Notably, in the PTAA case the QFLS and V_{OC} match, whereas for the P3HT the QFLS- V_{OC} mismatch is still present, consistently with the simulation in Figure S4C (Supporting Information). This gives strong empirical evidence that the saturation of the V_{OC} is caused by a recombination process related to the partial loss of selectivity of the hole-extracting contact and not to processes within the perovskite bulk. Possibly, a thicker HTL provides a better coverage of the indium-doped tin oxide (ITO) substrate, preventing direct accessibility of the minority carriers (electrons) to the wrong contact, either by direct contact, by tunneling, or through additional states caused by the interaction between the ITO substrate and the perovskite. Additionally, a thicker polymeric layer can form a smoother surface, reducing the perovskite crystal strain and the probability to have nonideal crystal formation at the interface, which can conceivably lead to interfacial defects above the perovskite bandgap.^[40,41] This finding indicates that, from an energetic point of view, the selectivity of the HTL used in this work is itself sufficient to block the minority carriers and it's not responsible for the saturation of the V_{OC} .

3.4. Device Picture

The two regions identified during the analysis of the *internal* and *external* ideality factor in devices with optimized, extremely

thin (<10 nm) transport layers represent essentially two different types of recombination mechanisms. Generally, when the $n_{id,ext}$ and $n_{id,int}$ are equal it means that the recombination processes affect the QFLS and the V_{OC} in a very similar way. On the other hand, the transition of $n_{id,ext}$ toward lower values, compared to $n_{id,int}$, implies the presence of an additional recombination pathway near or at the perovskite/TL interface that has a much larger effect on the V_{OC} compared to the QFLS. In this case the extra recombination pathway depletes the carrier reservoir near the perovskite surface faster than it can be replenished from the bulk by photogenerated carriers. As the hole current density toward the contact is given by $J = n_h \mu_h \nabla E_{F,h}$ (with μ_h the hole mobility), the upward bending of $E_{F,h}$ increases if the hole density in the perovskite near the HTL decreases, e.g. due to rapid hole recombination. This is the situation realized in the sample with a P3HT as HTL. **Figure 5** visualizes schematically the relation between the QFLS and the V_{OC} for different illumination condition in the different type of devices, based on the results of our drift-diffusion simulations in Figure S3C (Supporting Information). The scheme clearly shows that the quasi-Fermi levels $E_{F,e}$ and $E_{F,h}$ propagate flat throughout the bulk of the absorber, but significant bending at the perovskite/HTL interface can occur. This process results eventually in a lower V_{OC} and a consequent mismatch with the QFLS in the bulk, and the consequent failure of the S.Q. theory. This picture strongly highlights that the V_{OC} cannot always be truly representative of the recombination mechanisms occurring in the absorber and at its surfaces, but can lead to a misinterpretation of the recombination behavior. Additionally, this knowledge can be utilized for future solar cell improvement and development of new transporting layers strategies. In order to exploit the full potential of the material, these additional losses must be eliminated, especially for operational conditions at high carrier concentration. We propose that a perfectly aligned and fully blocking transport layer, which completely prevent the accessibility of the minority carriers and does not introduce an energetic offset for the majority carriers, is able to prevent the V_{OC} saturation until relatively high intensity and to nullify the QFLS- V_{OC} mismatch.

4. Conclusions

In summary, we characterized via intensity-dependent PLQY and V_{OC} measurements two perovskite pin solar cell model systems, utilizing PTAA and P3HT as HTL, and modelled the origin of the energy losses. We were able to compare the evolution of the *internal* QFLS and the *external* V_{OC} of the same working device with respect to the illumination intensity and their respective *internal* and *external* ideality factors. This allowed us to assign the dominant recombination pathways and how they affect the QFLS and V_{OC} in dependence of illumination intensities. For low and intermediate intensities, both quantities display a similar dependence on intensity, with values of the ideality factor between 1.3 and 1.5. We show by drift-diffusion simulations that these experimental findings are consistent with predominant trap-assisted recombination at the interfaces between the perovskite and the charge transporting layers, while little or no information can be drawn from n_{id} on

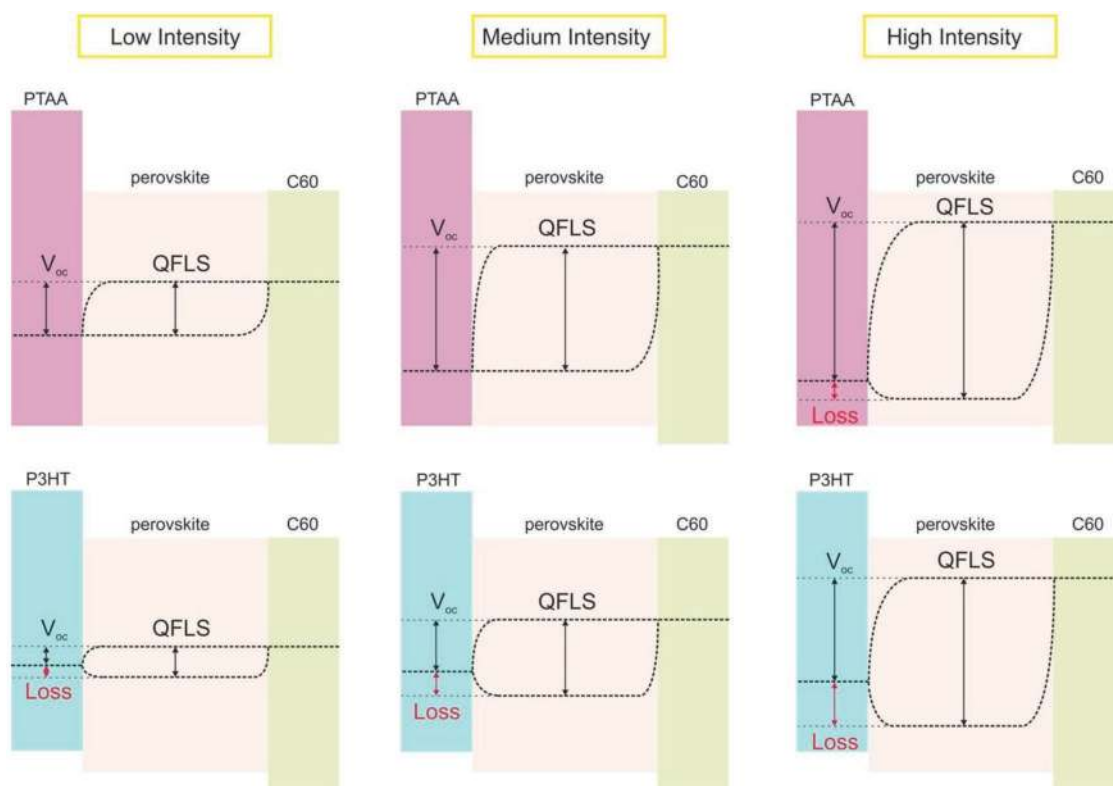


Figure 5. Schematic representation of the relation between the QFLS and the V_{OC} for different illumination intensities in the solar cells employing P3HT and PTAA as hole transport layer. The schemes have been derived from the results of drift-diffusion simulations in Figure S3c (Supporting Information). The dashed lines in the perovskite layer represent the $E_{F,e}$ and $E_{F,h}$ defining the QFLS, whereas the external V_{OC} is given by the respective energy levels at the contacts. The graph highlights the detrimental effects of P3HT on the V_{OC} of the cell, especially at high illumination intensities.

the rate and importance of radiative and trap-assisted recombination in the bulk. For the poorer performing cell with a P3HT HTL, we measure a large mismatch between the QFLS and the V_{OC} , which is consistently explained by an energetic offset between the perovskite and the transport layer in combination with faster interfacial recombination. Going to higher intensities, devices with a thin P3HT or PTAA HTL display a saturation of the V_{OC} but not of the QFLS. Temperature-related effects are safely excluded as a predominant cause for the V_{OC} saturation. Instead, our drift-diffusion simulations identify a reduced selectivity of the hole-extracting contact as being the major reason for the saturation of the V_{OC} at high intensities. In our cells, this extra loss channel can be fully suppressed by using thicker transport layers, thereby placing a thick enough wider bandgap layer between the perovskite and the ITO anode. It is only in this situation that our devices exhibit nearly identical values of the *internal* and *external* ideality factors. In conclusion, this work highlights how transport layers and their interfaces to the perovskite layer (and possibly electrode) govern the recombination behavior and the energy losses in perovskite solar cells. We also show that the V_{OC} may differ significantly from the QFLS in the perovskite bulk. As such, and given the multi-layer architecture of these devices, the recombination analysis from parameters obtained from electrical measurements, such as the V_{OC} , are not always truly representative of the processes occurring in perovskite absorber. The methodology proposed in

this work constitutes a relatively simple and reliable approach to investigate the true nature of the recombination of charges in complex device architecture, providing essential information about the physics in these complex devices.

5. Experimental Section

Device Preparation: Patterned ITO (Lumtec, 15 ohm sq^{-1}) was washed with acetone, Hellmanex III, DI-water, and isopropanol. After microwave plasma treatment (3 min at 200 W), PTAA (Sigma-Aldrich, $M_n = 7000\text{--}10\,000$, PDI = 2–2.2) in a concentration of 1.5 mg mL^{-1} was spin-coated at 6000 rpm for 30 s and immediately annealed for 10 min at 100 °C. After that, a 60 μL solution of PFN-P2 (0.5 mg mL^{-1} in methanol) was added onto the spinning substrate at 5000 rpm for 20 s resulting in a film with a thickness below the detection limit of the atomic force microscopy (AFM) (<5 nm). In the case of P3HT, an HTL (Sigma-Aldrich, $M_n \approx 27\,000$) was spin-coated from a 3 mg mL^{-1} DCB solution at 3000 rpm for 30 s (acceleration 3000 rpm s^{-1}) and subsequently annealed at 100 °C for 10 min. P3HT films were also oxygen plasma treated for 5 s to ensure sufficient wetting of the perovskite as discussed in a previous work.^[42] When thicker HTLs were prepared, PTAA and P3HT solution was used with higher concentration, 10 and 15 mg mL^{-1} , respectively, and spin-coated at slower rpm, 1500 rpm. The perovskite layer was formed by spin coating a DMF:DMSO solution (4:1 volume) at 4500 rpm for 35 s. After 10 s of spin coating, 500 mL of diethyl ether (antisolvent) was dripped on top of the spinning substrate. After spin coating, samples were annealed at 100 °C for 1 h. Afterward, samples were transferred to an evaporation chamber and C_{60} (30 nm), BCP (8 nm), and copper

(100 nm) were deposited under vacuum ($p = 10^{-7}$ mbar). The active area was 6 mm² defined as the overlap of ITO and the top electrode.

Current-Density–Voltage Characteristics and EQE_{pv}: *J–V* curves were measured under N₂ on a Keithley 2400 system in a two-wire configuration with a scan speed of 0.1 V s⁻¹ and voltage step of 0.02 V. One sun illumination at ≈100 mW cm⁻² of AM1.5G irradiation was provided by an Oriol class ABA sun simulator. The real illumination intensity was monitored during the measurement using a Si photodiode and the exact illumination intensity was used for efficiency calculations. The sun simulator was calibrated with a KG5 filtered silicon solar cell (certified by Fraunhofer ISE). The AM1.5G short-circuit current of devices matched the integrated product of the EQE spectrum within 5–10% error. The latter was recorded using a home-built set-up utilizing a Philips Projection Lamp (Type7724 12 V 100 W) in front of a monochromator (Oriol Cornerstone 74100) and the light was mechanically chopped at 70 Hz. The photogenerated current was measured using a lock-in-amplifier (EG&G Princeton Applied Research Model 5302, integration times 300 ms) and evaluated after calibrating the lamp spectrum with a UV-enhanced Si photodetector (calibrated at Newport).

Absolute Photoluminescence: Excitation for the PL measurements was performed with a 445 nm CW laser (Insaneware) through an optical fibre into an integrating sphere. The intensity of the laser was adjusted to a 1 sun equivalent intensity by illuminating a 1 cm² size perovskite solar cell under short-circuit and matching the current density to the *J*_{SC} under the sun simulator (22.0 mA cm⁻² at 100 mW cm⁻², or 1.375×10^{21} photons m⁻² s⁻¹). A second optical fiber was used from the output of the integrating sphere to an Andor SR393i-B spectrometer equipped with a silicon CCD camera (DU420A-BR-DD, iDus). The system was calibrated by using a calibrated halogen lamp with specified spectral irradiance, which was shone into to integrating sphere. A spectral correction factor was established to match the spectral output of the detector to the calibrated spectral irradiance of the lamp. The spectral photon density was obtained from the corrected detector signal (spectral irradiance) by division through the photon energy (*hf*), and the photon numbers of the excitation and emission obtained from numerical integration using Matlab. In a last step, three fluorescent test samples with high specified PLQY (≈ 70%) supplied from Hamamatsu Photonics where measured where the specified value could be accurately reproduced within a small relative error of less than 5%.

Measurement Conditions: All PL measurements were performed on complete cells, prepared fresh, and immediately encapsulated in a glove box under N₂ atmosphere. The PL of the samples was readily recorded after mounting the sample and after an exposure of 1 s at each laser intensity, after that the incident laser was blocked by a shutter and the next intensity adjusted while the sample was kept in dark conditions avoiding any effects induced by constant illumination. The cell was illuminated from the bottom glass/ITO. It is noted that all absolute PL measurements were performed on films with the same HTL, ETL, and perovskite thicknesses as used in the operational solar cells.

Intensity-Dependent V_{OC}: Intensity-dependent V_{OC} measurements were performed illuminating the respective solar cell exactly at the same illumination condition and exposure time (1 s) as during the PL measurements in order to have the same experimental condition for the two measurements. After each measurement the incident light was blocked with a shutter and the next light intensity adjusted. The corresponding V_{OC} was monitored with Keithley 2400 system in a two-wire configuration.

SCAPS Simulations: Simulation parameters and further details are discussed in Table S1 (Supporting Information). SCAPS is an open-source code and can be obtained from <https://users.elis.ugent.be/ELISgroups/solar/projects/scaps> upon the conditions requested by the developers Marc Burgelman et al.

Supporting Information

Supporting Information is available from the Wiley Online Library or from the author.

Acknowledgements

S.A. acknowledges funding from the German Federal Ministry of Education and Research (BMBF), within the project “Materialforschung für die Energiewende” (grant no. 03SF0540), and the German Federal Ministry for Economic Affairs and Energy (BMWi) through the “PersiST” project (grant no. 0324037C). Additional funding came from HyPerCells (a Joint Graduate School of the Potsdam University and the HZB) and by the Deutsche Forschungsgemeinschaft (DFG, German Research Foundation) – Project-ID 182087777 – SFB 951.

Conflict of Interest

The authors declare no conflict of interest.

Keywords

electro-optical materials, perovskite solar cells, photovoltaic devices, thin films

Received: May 20, 2019

Revised: June 16, 2019

Published online: July 25, 2019

- [1] G. Hodes, *Science* **2013**, *342*, 317.
- [2] Q. Dong, Y. Fang, Y. Shao, P. Mulligan, J. Qiu, L. Cao, J. Huang, *Science* **2015**, *347*, 967.
- [3] S. D. Stranks, G. E. Eperon, G. Grancini, C. Menelaou, M. J. P. Alcocer, T. Leijtens, L. M. Herz, A. Petrozza, H. J. Snaith, *Science* **2013**, *342*, 341.
- [4] W.-J. Yin, T. Shi, Y. Yan, *Appl. Phys. Lett.* **2014**, *104*, 063903.
- [5] I. L. Braly, D. W. Dequilettes, L. M. Pazos-Outón, S. Burke, M. E. Ziffer, D. S. Ginger, H. W. Hillhouse, *Nat. Photonics* **2018**, *12*, 355.
- [6] W. Tress, *Adv. Energy Mater.* **2017**, *7*, 1602358.
- [7] D. Shi, V. Adinolfi, R. Comin, M. Yuan, E. Alarousu, A. Buin, Y. Chen, S. Hoogland, A. Rothenberger, K. Katsiev, Y. Losovyj, X. Zhang, P. A. Dowben, O. F. Mohammed, E. H. Sargent, O. M. Bakr, *Science* **2015**, *347*, 519.
- [8] Y. Yang, M. Yang, D. T. Moore, Y. Yan, E. M. Miller, K. Zhu, M. C. Beard, *Nat. Energy* **2017**, *2*, 16207.
- [9] X. Zheng, B. Chen, J. Dai, Y. Fang, Y. Bai, Y. Lin, H. Wei, X. C. Zeng, J. Huang, *Nat. Energy* **2017**, *2*, 17102.
- [10] D. Y. Son, J. W. Lee, Y. J. Choi, I. H. Jang, S. Lee, P. J. Yoo, H. Shin, N. Ahn, M. Choi, D. Kim, N. G. Park, *Nat. Energy* **2016**, *1*, 16081.
- [11] M. Stolterfoht, C. M. Wolff, J. A. Márquez, S. Zhang, C. J. Hages, D. Rothhardt, S. Albrecht, P. L. Burn, P. Meredith, T. Unold, D. Neher, *Nat. Energy* **2018**, *3*, 847.
- [12] M. Stolterfoht, P. Caprioglio, C. M. Wolff, J. A. Márquez, J. Nordmann, S. Zhang, D. Rothhardt, U. Hörmann, A. Redinger, L. Kegelmann, S. Albrecht, T. Kirchartz, M. Saliba, T. Unold, D. Neher, *Energy Environ. Sci.* **2018**, <http://doi.org/10.1039/C9EE02020A>.
- [13] P. Caprioglio, F. Zu, C. M. Wolff, J. A. M. Prieto, M. Stolterfoht, N. Koch, T. Unold, B. Rech, S. Albrecht, D. Neher, *Sustainable Energy Fuels* **2019**, *3*, 550.
- [14] C. M. Wolff, F. Zu, A. Paulke, L. P. Toro, N. Koch, D. Neher, *Adv. Mater.* **2017**, *29*, 1700159.
- [15] K. Tvingstedt, C. K. Deibel, *Adv. Energy Mater.* **2016**, *6*, 1502230.
- [16] T. Kirchartz, U. Rau, *Phys. Status Solidi A* **2008**, *205*, 2737.
- [17] W. Tress, M. Yavari, K. Domanski, P. Yadav, B. Niesen, J. P. Correa Baena, A. Hagfeldt, M. Graetzel, *Energy Environ. Sci.* **2018**, *11*, 151.

- [18] M. Wolf, H. Rauschenbach, *Adv. Energy Convers.* **1963**, 3, 455.
- [19] P. Würfel, *J. Phys. C: Solid State Phys.* **1982**, 15, 3967.
- [20] W. Shockley, H. J. Queisser, *J. Appl. Phys.* **1961**, 32, 510.
- [21] Z. Wang, Q. Lin, B. Wenger, M. G. Christoforo, Y. H. Lin, M. T. Klug, M. B. Johnston, L. M. Herz, H. J. Snaith, *Nat. Energy* **2018**, 3, 855.
- [22] S. W. Glunz, J. Nekarda, H. Mäckel, A. Cuevas, *Proc. 22nd Eur. Photovoltaic Sol. Energy Conf.*, Milan, Italy, September **2007**, pp 849–853.
- [23] O. Gunawan, T. Gokmen, D. B. Mitzi, *J. Appl. Phys.* **2014**, 116, 084504.
- [24] V. Sarritzu, N. Sestu, D. Marongiu, X. Chang, S. Masi, A. Rizzo, S. Colella, F. Quochi, M. Saba, A. Mura, G. Bongiovanni, *Sci. Rep.* **2017**, 7, 44629.
- [25] T. Unold, L. Gütay, in *Advanced Characterization Techniques for Thin Film Solar Cells*, 1st ed. (Eds: D. Abou-Ras, T. Kirchartz, U. Rau), Wiley VCH, Weinheim, Germany **2011**, pp. 151–175.
- [26] G. H. Bauer, L. Gütay, R. Kniese, *Thin Solid Films* **2005**, 480–481, 259.
- [27] G. El-Hajje, C. Momblona, L. Gil-Escrig, J. Ávila, T. Guillemot, J.-F. Guillemoles, M. Sessolo, H. J. Bolink, L. Lombez, *Energy Environ. Sci.* **2016**, 131, 6050.
- [28] I. L. Braly, H. W. Hillhouse, *J. Phys. Chem. C* **2016**, 120, 893.
- [29] U. Rau, *Phys. Rev. B* **2007**, 76, 085303.
- [30] M. Saliba, T. Matsui, J.-Y. Seo, K. Domanski, J.-P. Correa-Baena, M. K. Nazeeruddin, S. M. Zakeeruddin, W. Tress, A. Abate, A. Hagfeldt, M. Grätzel, *Energy Environ. Sci.* **2016**, 9, 1989.
- [31] M. Stolterfoht, C. M. Wolff, Y. Amir, A. Paulke, L. Perdígón-Toro, P. Caprioglio, D. Neher, *Energy Environ. Sci.* **2017**, 10, 1530.
- [32] F. Staub, H. Hempel, J. Hebig, J. Mock, U. W. Paetzold, U. Rau, T. Unold, T. Kirchartz, *Phys. Rev. Appl.* **2016**, 6, 044017.
- [33] J. M. Richter, M. Abdi-Jalebi, A. Sadhanala, M. Tabachnyk, J. P. H. Rivett, L. M. Pazos-Outón, K. C. Gödel, M. Price, F. Deschler, R. H. Friend, *Nat. Commun.* **2016**, 7, 13941.
- [34] T. Kirchartz, B. E. Pieters, J. Kirkpatrick, U. Rau, J. Nelson, *Phys. Rev. B* **2011**, 83, 1.
- [35] C. Van Berkel, M. J. Powell, A. R. Franklin, I. D. French, *J. Appl. Phys.* **1993**, 73, 5264.
- [36] M. B. Johnston, L. M. Herz, *Acc. Chem. Res.* **2015**, 146.
- [37] S. D. Stranks, V. M. Burlakov, T. Leijtens, J. M. Ball, A. Goriely, H. J. Snaith, *Phys. Rev. Appl.* **2014**, 2, 034007.
- [38] G. J. A. H. Wetzelaer, M. Scheepers, A. M. Sempere, C. Momblona, J. Ávila, H. J. Bolink, *Adv. Mater.* **2015**, 27, 1837.
- [39] S. Ullbrich, A. Fischer, Z. Tang, J. Ávila, H. J. Bolink, S. Reineke, K. Vandewal, *Phys. Rev. Appl.* **2018**, 9, 051003.
- [40] S. Olthof, K. Meerholz, *Sci. Rep.* **2017**, 7, 40267.
- [41] F. Wang, S. Bai, W. Tress, A. Hagfeldt, F. Gao, *npj Flexible Electron.* **2018**, 2, 22.
- [42] S. Zhang, M. Stolterfoht, A. Armin, Q. Lin, F. Zu, J. Sobus, H. Jin, N. Koch, P. Meredith, P. L. Burn, D. Neher, *ACS Appl. Mater. Interfaces* **2018**, 10, 21681.